TÜBİTAK

Turkish Journal of Earth Sciences

http://journals.tubitak.gov.tr/earth/

Research Article

Turkish J Earth Sci
(2023) 32: 200-213
© TÜBİTAK
doi:10.55730/1300-0985.1838

Lithological mapping of ophiolitic rocks from southern part of the Sivas Basin (Turkey) using ASTER imagery

Taner EKİCİ*
Department of Geological Engineering, Sivas Cumhuriyet University, Sivas, Turkey

Received: 02.07.2022 • **Accepted/Published Online:** 03.12.2022 • **Final Version:** 27.03.2023

Abstract: The east-west extended Sivas Basin in central-eastern Anatolia is a foreland basin that formed after the obduction of the Tethyan ophiolite during the late Cretaceous and is also a north-verging fold-and-thrust belt. The basement rocks of the basin represent mainly sedimentary (Mesozoic platform-type carbonates) and late Cretaceous Divriği ophiolitic complex. As the ophiolitic rocks are affected by intense tectonic processes, field-based mapping studies require long processes and costs. The study tests to reveal the lithological features of the ophiolitic complex outcropping around the Ulaş district of the Sivas Province using remote sensing methods and techniques. Due to arid climatic conditions and rare vegetation cover in the region, almost all outcrops of the basin rocks can be separated by spectral enhancement methods easily. Band ratio (BR), spectral indices (SI), decorrelation stretch (DS), principal component analysis (PCA), and support vector machine (SVM) on Advanced Spaceborne Thermal Emission and Reflection Radiometer (ASTER) data were used in this research. BR, PCA, DC, and SI techniques clearly distinguish the Divriği Ophiolitic Complex from the basement and cover sedimentary rocks. SVM distinguishes the chromite-bearing dunites from the other ophiolite-related rock units. According to image analysis performances, it has been observed that the rocks of the Divriği ophiolitic complex can be differentiated in more detail compared to a 1/100.000 scaled geological map of the region.

Key words: Lithological mapping, image processing, ASTER, multispectral, Central Anatolia

1. Introduction

Mapping of ophiolitic sequences has become a research interest of scientists and exploration geologists around the world (Xiong et al., 2011; Eslami et al., 2015; Emam et al., 2016; Zhang and Zeng, 2018; Abrams and Yamaguchi, 2019; Rajendran and Nasir, 2019; Çörtük et al., 2020; Ahmadi and Kalkan, 2021; Traore et al., 2022). An ideal ophiolitic rock sequence begins with ultramafic rocks at the bottom and ends with basic transition zone rocks, then a mafic gabbro sequence, sheeted diabase dykes, pillow lava and epiophiolitic cover rocks overlying them (e.g., Moores, 1982; Pearce, 2008; Dilek and Furnes, 2011). Ophiolitic rocks are potential areas for many ore deposits as well. Especially important mineral deposits such as chromite, copper, gold, silver, magnesite, sepiolite, nickel, talc, and asbestos are associated with ophiolitic rocks. Ophiolitic rocks are widely exposed in Alpine-Himalayan Orogenic Belt from the western of Turkey to Tibet. The ophiolites crop out in east-west trending suture zones from north to south in Turkey (Figure 1) and are interpreted to have formed in a supra-subduction zone (SSZ) tectonic setting (Parlak et al., 2002; Çelik et al., 2013; Parlak et al., 2013; Topuz et al., 2013; Uysal et al., 2015; Özkan et al., 2020). Chromite mineralization is widespread in the number of regions, namely Eskişehir-Kütahya-Bursa in northwest Anatolia, Fethiye-Köyceğiz-Denizli in western Taurides, Adana-Mersin, İskenderun-Hatay-Gaziantep in the south-southeast, Elazığ and Sivas-Erzincan regions in the east and northeast of Turkey (Pearce et al., 1984; Parlak, 1996; Parlak et al., 1996, 2000, 2002, 2004, 2006; Yalınız et al., 1996, 2000; Beyarslan and Bingöl, 2000; Floyd et al., 2000; Robertson, 2002, 2004; Çelik and Delaloye, 2003; Kavak et al., 2017). The Divriği region in east-central Anatolia comprises the Tauride platform unit, ophiolitic melange, ophiolite-related metamorphic rocks, ophiolitic rocks, a volcano-sedimentary unit, granitoid rocks, and Tertiary cover sediments (Parlak et al., 2006). Geochemical evidence from previous studies suggests that the late Cretaceous Divriği ophiolite formed in a suprasubduction zone tectonic setting to the north of the Tauride platform (Parlak et al., 2006; Kavak et al., 2017). The Divriği ophiolite in the southern part of Sivas (Turkey) possesses abundant chromite mineralizations which are actively mined. The chromite deposits are mainly podiform in type

* Correspondence: tanere@cumhuriyet.edu.tr

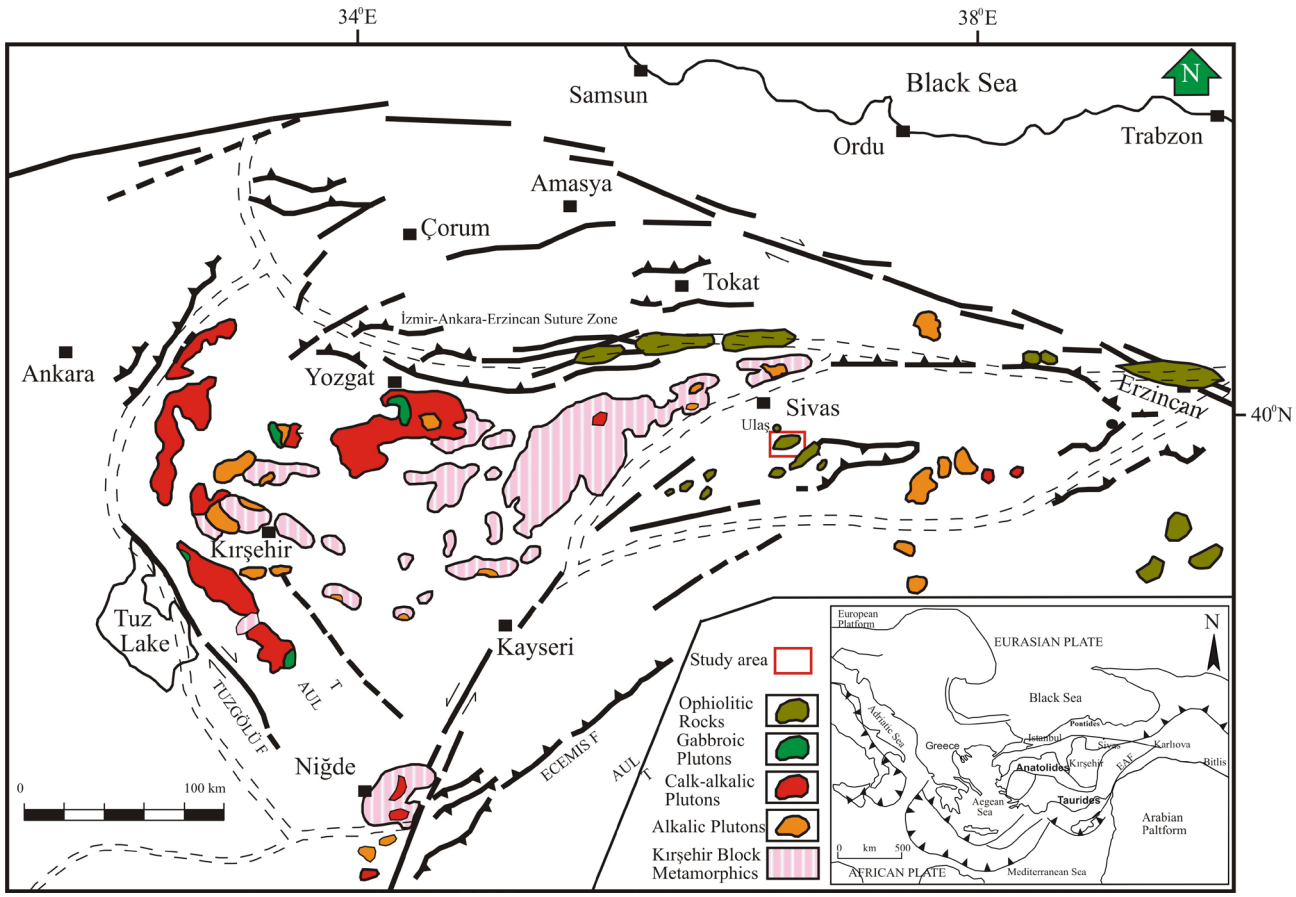

Figure 1. Tectonic map of Turkey and location of the study area (modified from Okay and Tüysüz, 1999).

and observed within the MOHO transition zone in the mantle tectonites. As known, the produced 57.4% of the total chromite ore in the world is produced from podiform deposits (Mosier et al., 2012).

Remote sensing analysis plays an important role in the exploration of mineral deposits on Earth, as well as in lithological and mineral mapping and structural properties. The Advanced Spaceborne Thermal Emission and Reflection Radiometer (ASTER) is an instrument that ensures new applicable data for these properties (Amer et al., 2010; Hewson et al., 2005; Mohamed El-Desoky et al., 2021). It consists of three visible and near-infrared spectral bands (VNIR, between 0.52 and 0.86 µm, with 15 m spatial resolution), infrared reflecting radiation in six short wavelength infrared spectral bands (SWIR, between 1.6 and 2.43 µm, with 30 m spatial resolution), and thermal reflecting radiation in 5 thermal infrared bands (TIR, between 8.125 and 11.65 µm, with 90 m spatial resolution). It has a 60 km swath width (Url-1).

There exist three main important tectonic units in Sivas and around the region (Figure 1). These tectonic units are represented by the Pontide Tectonic Belt, the North Anatolian Ophiolite Belt and the Tauride Tectonic Belt, from north to south (Yılmaz, 1989). Ophiolitic rocks are common in the study area. Due to the abundance of peridotites that host chromite deposits in the Divriği ophiolite, new chromite deposits are likely to be discovered and further research and investigation are needed. Since given the extremely rugged topography with difficult accessibility, remote sensing methods and techniques s can be useful for this purpose. This study aims to rock differentiation and the separation of chromite-bearing mineralization in the Divriği ophiolite complex using ASTER satellite data. A more scientific statement has been reported related to easily distinguishing various rocks and providing detailed geological maps of the ultramafic rocks (Kavak et al., 2010; Töre, 2010; Rajendran et al., 2012; Rowan and Mars, 2003).

A study using remote sensing technology and its terrestrial components was carried out by Gürsoy (2019) in the same study area. In that study, only the determination of dunite minerals in ultramafic rocks was carried out. As a result, in the study, a new band combination was obtained for the detection of only dunites, and the detection of

other ultramafic rocks was ignored. In this study, the use of existing remote sensing techniques, which will facilitate the detection of ophiolitic rocks in general ultramafic rocks, is discussed.

The image processing techniques such as band rationing (BR), spectral indices (SI), decorrelation stretch (DC), principal component analysis (PCA), and support vector machine (SVM) as spectral classification methods were applied in this study. This study tests the results of these remote sensing techniques and methods on the lithological mapping of the Divriği ophiolitic rocks and especially dunitic rocks which have the potential for economic chromite deposits.

2. Geological setting

Sivas Basin is located in the eastern part of Central Anatolia (Poisson et al., 1996; Kergaravat, 2016; Legeay, 2017) (Figure 1). The study area covers the Ulaş (Sivas) district and its surroundings located in the south-southeast of Sivas Basin. The most basic rocks consist of the late Triassic-late Cretaceous Munzur limestones, late Cretaceous Divriği Ophiolitic Complex, late Cretaceous-Paleocene Tecer Formation, Eocene Demiroluk Formation, Oligo-Miocene Yağbasan member of Demiroluk Formation, Oligo-Miocene Conglomerate member of Kemah Formation, middle-late Miocene Kavak Formation and early Pliocene Kangal Formation in the study area (Figure 2).

The late Triassic-late Cretaceous Munzur limestone consists of allochthonous, medium-thick bedded, gray-whitish, yellowish to cream-colored limestones. It is highly broken and cracked and its cracks are filled with secondary calcite. The thickness of the unit is between 400 and 750 m (Özgül et al., 1981). The late Cretaceous Divriği Ophiolite Complex overlies the Munzur limestones with a tectonic contact. The late Cretaceous Divriği Ophiolitic Complex consists of, from bottom to top, an ophiolitic melange, metamorphic sole, mantle tectonites, cumulates, isotropic gabbro, and sheeted dykes (Parlak et al., 2006; Kavak et al., 2017). The Tecer Formation unconformably overlies the ophiolite in the region. The late Cretaceous-Paleocene Tecer Formation consists of gray to blackish colored, medium-thick bedded cracked, micritic textured limestones containing abundant fossils shells (Inan and Inan, 1988). The Eocene Demiroluk Formation consists of clayey limestone, sandstone, and mudstone. This unit was deposited in the lagoon environment with abundant fossils and its thickness reaches up to 200 m (Özgül et al., 1973). The Oligo-Miocene Yağbasan member consisting of evaporites and olistoliths and a conglomerate of Kemah Formation overlies the Eocene units. The 800–900 m thick Yağbasan member was deposited in the shallow marine, lagoon, and terrestrial environments (Kurtman, 1973). It is observed in olistoliths of ophiolitic melange. The conglomerates of the Kemah formation with a thickness of 70–80 m are well–sorted (Kurtman, 1973). The middle-late Miocene Kavak Formation unconformably overlies the conglomerates. The Kavak formation consists of conglomerate, sandstone, and clayey limestone (Aktimur et al., 1990). This unit was horizontally bedded and mostly deposited in constant lake conditions and no fossil was

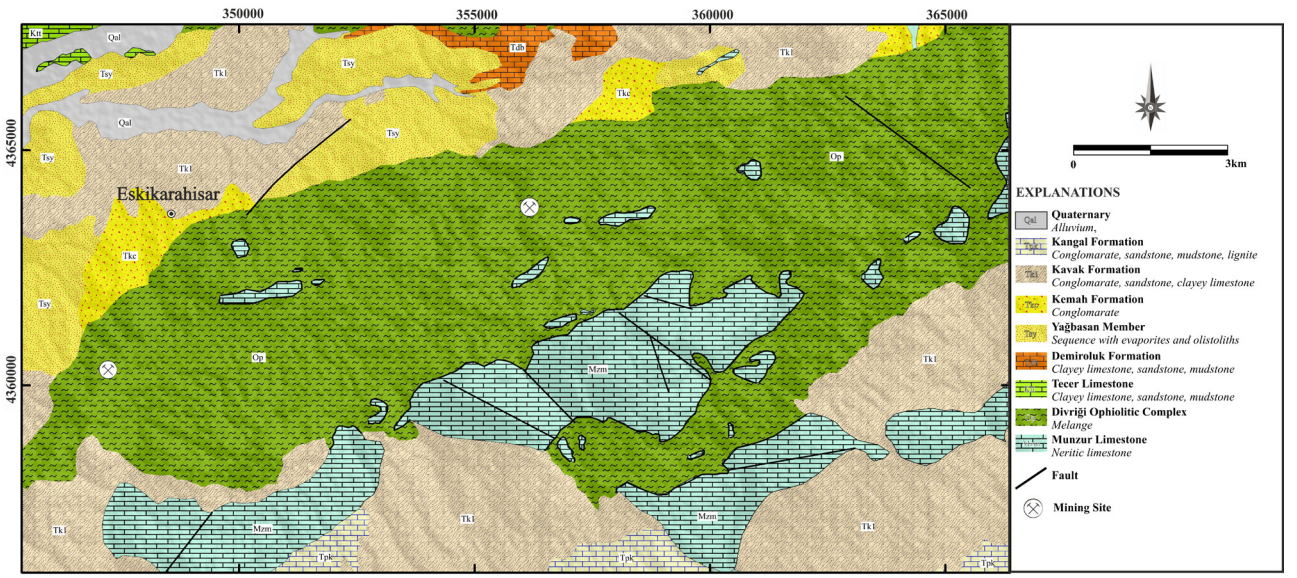

Figure 2. Local geological map of the study area (modified from Atabey ve Aktimur, 1997) (Mzm, Munzur Limestone; Op, Divriği Ophiolitic Complex; KTt, Tecer Formation; Tdb, Demiroluk Formation; Tsy, Demiroluk Formation Yağbasan Member; Tkc, Kemah Formation; Tk1, Kavak Formation; TPk, Kangal Formation; Qal, Alluvium).

documented in it. The early Pliocene Kangal Formation consists of conglomerate, sandstone, mudstone and lignite deposits. The 200 m thick unit having vertebrate fossils was also observed (Aktimur et al., 1988).

3. Material and methods

A number of samples from different ophiolite-related geological units (ultramafic rocks) in the study area were collected and prepared for petrographic examinations at Sivas Cumhuriyet University, Department of Geological Engineering Laboratories.

The ASTER level 1B data were used for the integration of field and laboratory studies. ASTER is a multispectral imaging sensor that measures electromagnetic radiation emitted and reflected from Earth's surface and atmosphere in 14 spectral bands The bands contain three visible and near-infrared radiation (VNIR) bands ranging between 0.52 and 0.86 μm with a spatial resolution of 15 m; six shortwave infrared radiation (SWIR) bands from 1.6 to 2.43 μm with a spatial resolution of 30 m; and five thermals infrared radiation (TIR) bands in the 8.125– 11.65 μm wavelength region with a spatial resolution of 90 m (Url-1) An additional backward-looking band in the visible and near-infrared radiation makes it possible to construct digital elevation models (DEM) from the view band 3N and back view band 3B. ASTER swath width is 60 km (each scene is 60 × 60 km) which makes it useful for regional mapping (Abrams, 2000; Rajendran et al., 2012; Yamaguchi et al., 1998).

3.1. Preprocessing of the ASTER data

In this study, ASTER data were obtained from the NASA Land Process Distributed Active Archive Center (LPDAAC) (Figure 3). ASTER L1B satellite data are produced without atmospheric/thermal corrections (Abrams, 2000). In addition, SWIR bands contain sensor errors. In order to increase the accuracy of the results obtained in image processing and spectral classification methods, these should be eliminated. In order to eliminate these effects, operations such as cross-talk correction radiance calibration and atmospheric were applied to the image. ERSDAC software was used for cross-mixing correction on the SWIR bands from 4 into bands 5 and 9, aimed at removing the effect of energy overspill. The software automatically applies the relationship proposed by (Iwasaki and Tonoka, 2005). Radiance calibration was applied by using (Abrams and Hook, 1995). The equation which is proposed by Archard and D'Souza (1994) and Eva and Lambin (1998) was used on the VNIR and SWIR bands for the atmospheric correction. ER MAPPER software was used in both processes and applied one by one to the bands belonging to the image. VNIR, SWIR, and TIR bands were corrected using MODTRAN-based atmospheric correction. The VNIR (15 m pixel size) bands were layer-stacked and resampled to 30 m spatial resolution to fit the SWIR bands for image processing.

3.2. Image processing for mapping

BR, SI, DS, PCA, and SVM methods were implemented to ASTER data in order to obtain the lithological mapping of ophiolitic and sedimentary rocks in the study area. BR is a very simple and powerful technique in order to emphasize the anomaly of the target objects. The technique is used to enhance the spectral differences between bands and to reduce the effects of topography in the raw images (Abdeen et al., 2001; Abrams et al., 1983; Hewson et al., 2001; Inzana et al., 2003; Rowan and Mars, 2003; Velosky et al., 2003). BR images are generated by dividing the brightness value in the band by numerical values in another band for each pixel. Some researchers have reported lithological mapping in ophiolite complexes by using BR (Abrams et al., 1983; Amer et al., 2010; Gabr et al., 2010; Gad and Kusky, 2007; Gürsoy, 2019; Khan and Mahmood, 2008; Ninomiya, 2003; Özkan et al., 2018; Pournamdari et al., 2014; Rajendran et al., 2012; Rowan and Mars, 2003). Several specialized band ratios have been applied to ASTER data, including (9/8, 4/3, 2/1 in the RGB (Rajendran et al., 2012).

SI is also utilized on ASTER TIR bands, including Quartz Index (QI)=(Band11×Band11)/(Band10×Band12), Carbonate Index (CI) =(Band13)/(Band14) and Mafic Index (MI)=(Band12)/(Band13) for lithological mapping in the arid and semiarid region (Ninomiya et al., 2005).

Decorrelation stretch is the most important image enhancement method to improve the visual interpretation of multispectral data sets (Gillespie et al., 1986). It has been successfully used for the mapping of ophiolitic rock complexes (Abrams and Hook, 1995).

PCA method is a conventional multivariable statistical analysis using orthogonal transform. A set of correlated variables is converted to a set of linearly uncorrelated principal components (PCs) in PCA (Pour and Hashim, 2011; Sabins, 1987). PCA is a well-known method for lithological and alteration mapping (Bennett et al., 1993; Cŕosta et al., 2003; Tangestani and Moore, 2001; Köküm, 2019; Zabcı, 2021). PCA was applied to proposed VNIR-SWIR ASTER bands.

SVM is a supervised classification method based on the statistical learning approach in multi- and hyperspectral data (Chapelle et al., 1999; Sain and Vapnik, 1996; Zhu and Blumberg, 2002). The representative lithological samples of different rocks were selected via regions interest (ROI) according to field surveys for SVM classification. Representative locations belonging to different rock outcrops, water, and vegetation in the study area were selected in order to reveal the spectral features (Figure 3).

4. Petrography

The collected representative ultramafic rock samples from the study area were defined to be serpentinized dunite, harzburgite, and pyroxenite as a result of petrographic examinations carried out under polarized microscopy.

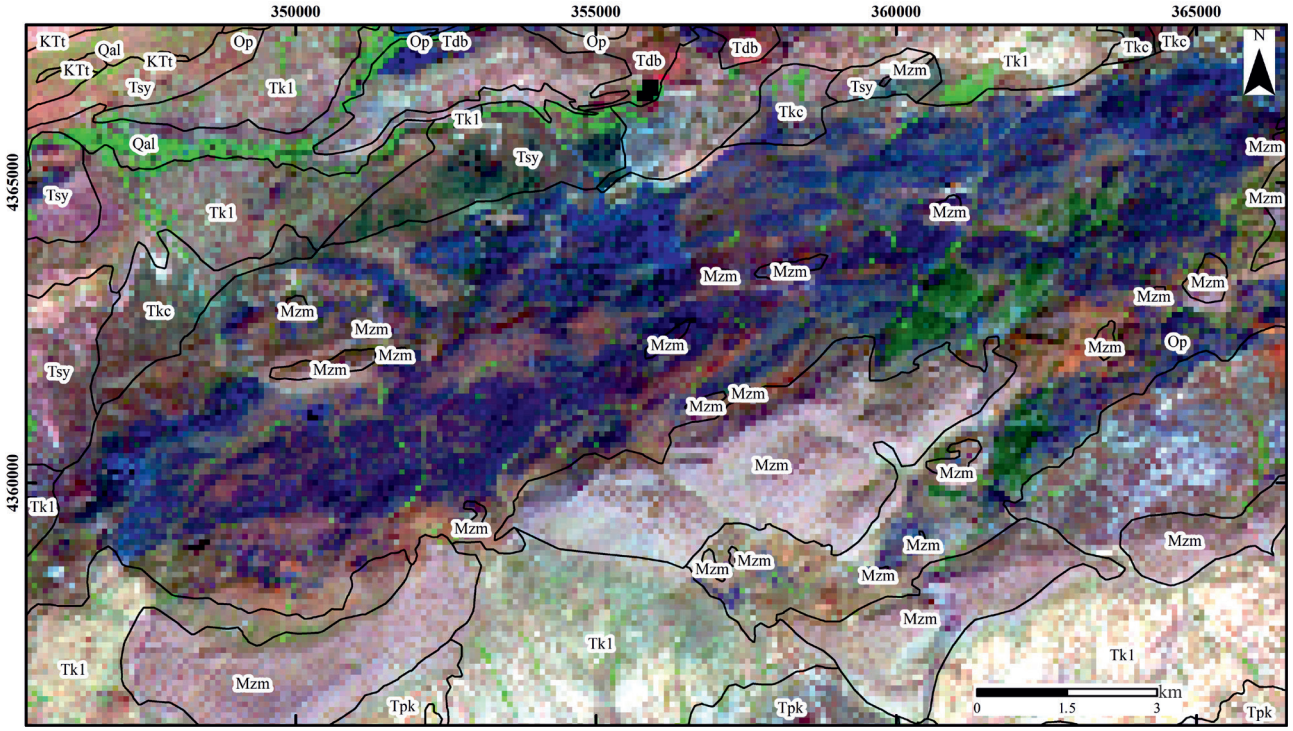

Figure 3. Simple color composite image of the study area R:8, G3, B:1 which is proposed by (Abrams et al., 1988; Rothery, 1987) (abbreviations are shown in Figure 2).

Ophiolitic rocks contain more than vol. 90% of mafic minerals such as olivine, pyroxene, and amphibole. More than vol. 90% of these mafic minerals in dunites are composed of olivines, while the majority of mafic minerals in harzburgite rocks are olivine, but there are also significant amounts of pyroxene minerals. In pyroxenites, more than vol. 90% of the minerals are pyroxene minerals. Serpentinized dunite samples are almost entirely composed of olivine minerals and chromite mineralization as opaque minerals, while harzburgite samples are mostly composed of olivine and less often orthopyroxene minerals and chromium mineralization as opaque minerals (Figures 4a–4d).

The Tecer Formation consists of interlayered carbonates as Tecer limestone and clastic sedimentary rocks as sandstones. The limestone includes microscopically intraclast, fossil and fossil shell fragments and grains that are connected to each other by a micritic matrix. The fractures and cracks observed in the rock are also filled with calcite (Figures 4e and 4f). The sandstones are fine to medium-grained and reddish in color. The petrographic investigations of the sandstones show that they deposit in shallow marine environments owing to bearing sparicalcite matrix, and consist of quartz, feldspar and rock fragments as granular components. The rock fragments are mostly characterized by limestone and ultramafic rocks. Siltstones are also medium to fine-grained and grey-white in color.

5. Results and discussions

Taking into account the necessary pretreatments and appropriate parameters, spatial remote sensing surveys can be very effective in terms of detecting outcrops and signs of alteration minerals on the surface. A major advantage of remote sensing data is that it provides a synoptic view over large areas that are impossible to measure using ground-based techniques. Although the use of optical sensors is limited and which sensors are suitable for which parameters, remote sensing offers a better understanding of ecological and biological relationships and processes, functions and dynamics. Remote sensing alone provides one-dimensional view of surveys and research, but when combined with ground-based datasets, it helps provide detailed results and critical analysis (Thakur et al., 2021).

Considering the limitations of doing fieldwork on the ground and the inability to master all the details of the terrain, remote sensing is a very useful technique in mineral targeting. Mineral deposits are associated with different geological environmental characteristics. Mineral determination in short time periods and at low costs using remote sensing technology is very useful compared to ground-based prospecting methods (Carranza, 2008).

In order to check the accuracy of the results of the methods applied to remote sensing data, a 1:100,000 scale reference geological map was used. It was understood that the results were compatible with the geological map, and

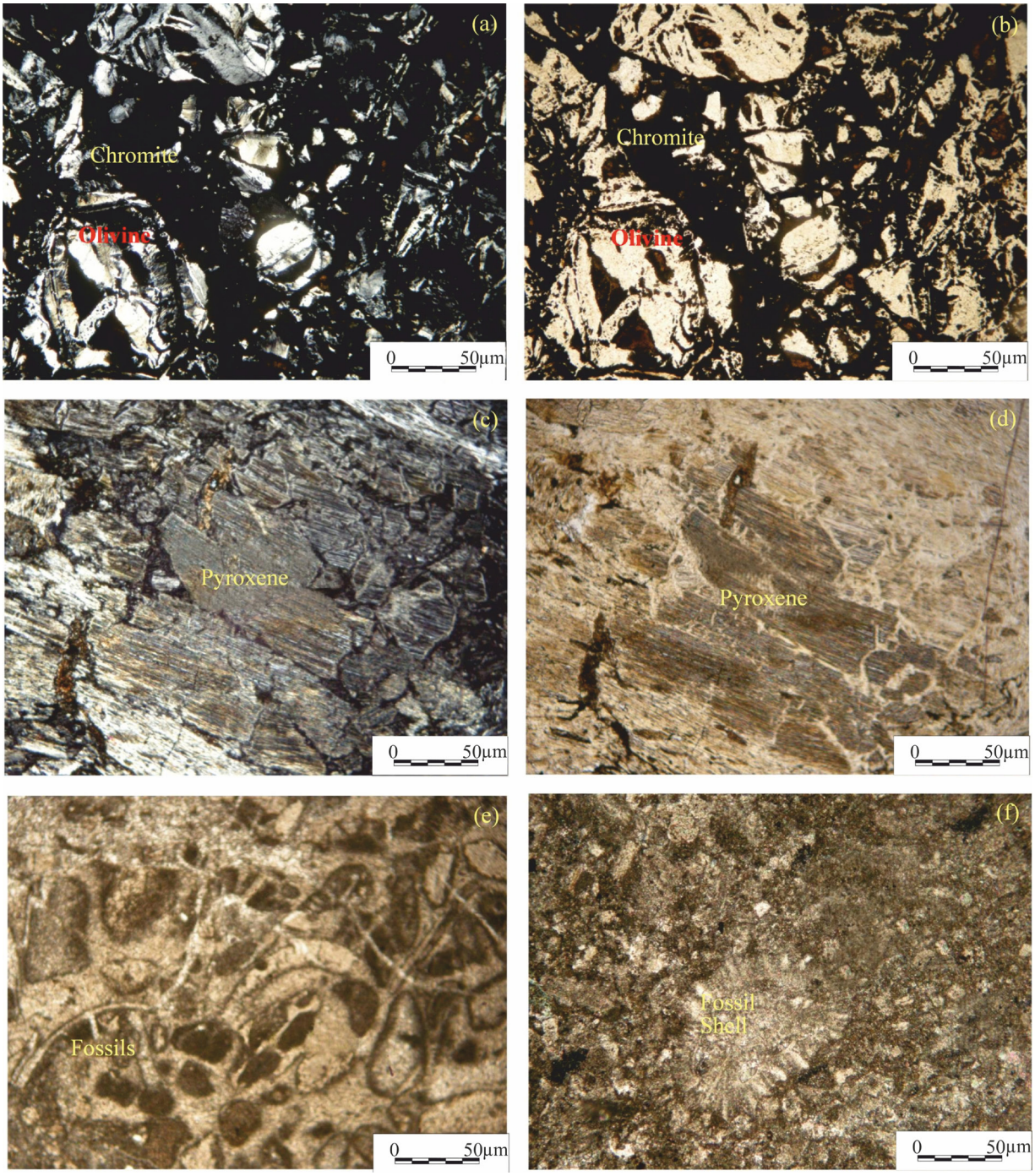

Figure 4. The photomicrographs of the different rocks from the study area. (a & b) Olivine and chromite in the dunit of the Divriği Ophiolitic Complex, (c & d) Pyroxene in the pyroxinite rocks of the Divriği Ophiolitic Complex, (e & f) Fossils and fossil shell in Limestones of the Tecer Formation.

it was evaluated that the applied methods gave successful results in the detection of ophiolite rocks.

5.1. Band ratio

Band ratio depends on the division of one spectral band to another in a multioptical scene. This division gives the ratio of the spectral reflectance measured in one spectral band to the spectral reflectance measured in another. Thus, the band scale technique highlights spectral differences associated with specific materials to be mapped and separates these surface materials from each other;

otherwise, this information will not be available in a band (Jensen, 1996). The resulting image is grayscale and to improve display quality across the 256 grayscale range, it is stretched. The best stretching method used for the scale images here in this study is contrast normalized stretching. RGB band ratios such as (9/8,4/3, and 2/1) and (4/8, 4/1 and 3/2*4/3) on ASTER imagery which is proposed by Rajendran and Nasir (2015, 2019) for discrimination of the ophiolitic and sedimentary rocks were applied in this study.

According to the RGB (9/8,4/3 and 2/1) band ratio image in this study, the ophiolitic rocks represented by serpentinized ultramafic rocks (harzburgite and dunite) have appeared in a yellowish to purplish color, while the limestone has a light bluish color, and claystone, sandstone, and siltstone have dark greenish to reddish colors (Figure 5).

A better-detailed image to distinguish the lithological units was obtained by applying the band ratios as 4/8, 4/1, and 3/2*4/3. Especially, the serpentinized dunite (reddish color) and harzburgite (light bluish color) have been discriminated from the sedimentary rocks in this band ratio image (Figure 6).

5.2. Spectral indices (SI)

In order to distinguish mafic-ultramafic and sedimentary rocks such as harzburgite, serpentinized dunite, limestone, sandstone, and siltstone exposed in the study area, index methods (Ninomiya et al., 2005) have been applied to ASTER TIR bands. MI (mafic index), CI (carbonate index), and QI (quartz index) in the RGB image have been created with false color composition (Figure 7). Ophiolites have been discriminated from the sedimentary rocks in this figure. Especially, the serpentinized dunite has a dark pinkish color, while the harzburgite has dark bluish color. The limestone also has a yellowish color.

5.3. Decorrelation stretch (DS)

Very faint pictographs almost invisible to the eye could be brought out by using DS. Conspicuous differences in hue which could give clues to superposition are enhanced. Pictographs can be enhanced for publication or presentation to viewers not capable (or inclined) to puzzle out faint elements. The use of DS can be as simple as just hitting a button, but it also contains sophisticated tools for the manipulation of false color images. Because the enhancement works by increasing differences in hue, the technique gives better results for pictographs than petroglyphs.

DS has been applied to 1-2-3 ASTER VNIR bands. According to Figure 8, the ophiolitic rocks have distinctly differentiated from the sedimentary rocks. Serpentinized dunite and harzburgite appeared together as greenish to reddish colors.

5.4. Principal component analysis (PCA)

PCA has been applied to ASTER VNIR-SWIR bands. Three principal components (PC4, PC5, and PC1) in the false color composition have been generated for discrimination

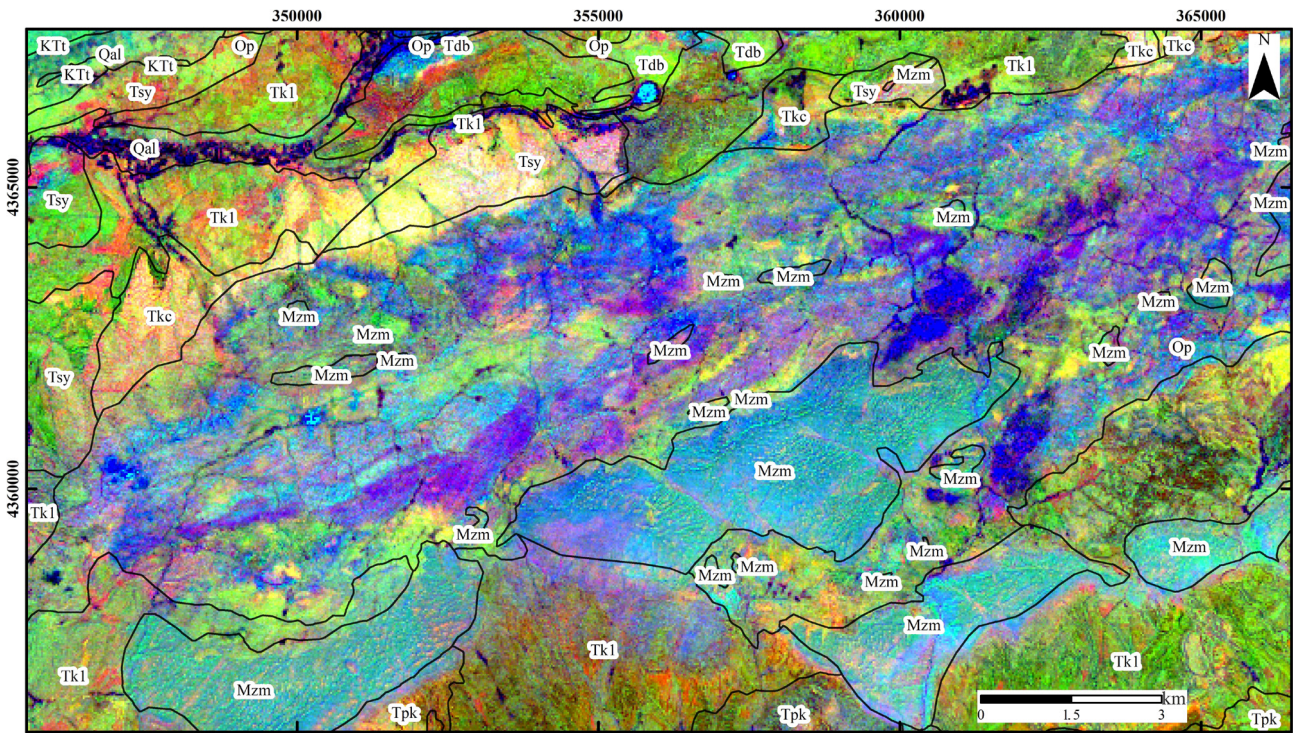

Figure 5. The band ratio image (9/8, 4/3, and 2/1 in the RGB) (abbreviations are shown in Figure 2).

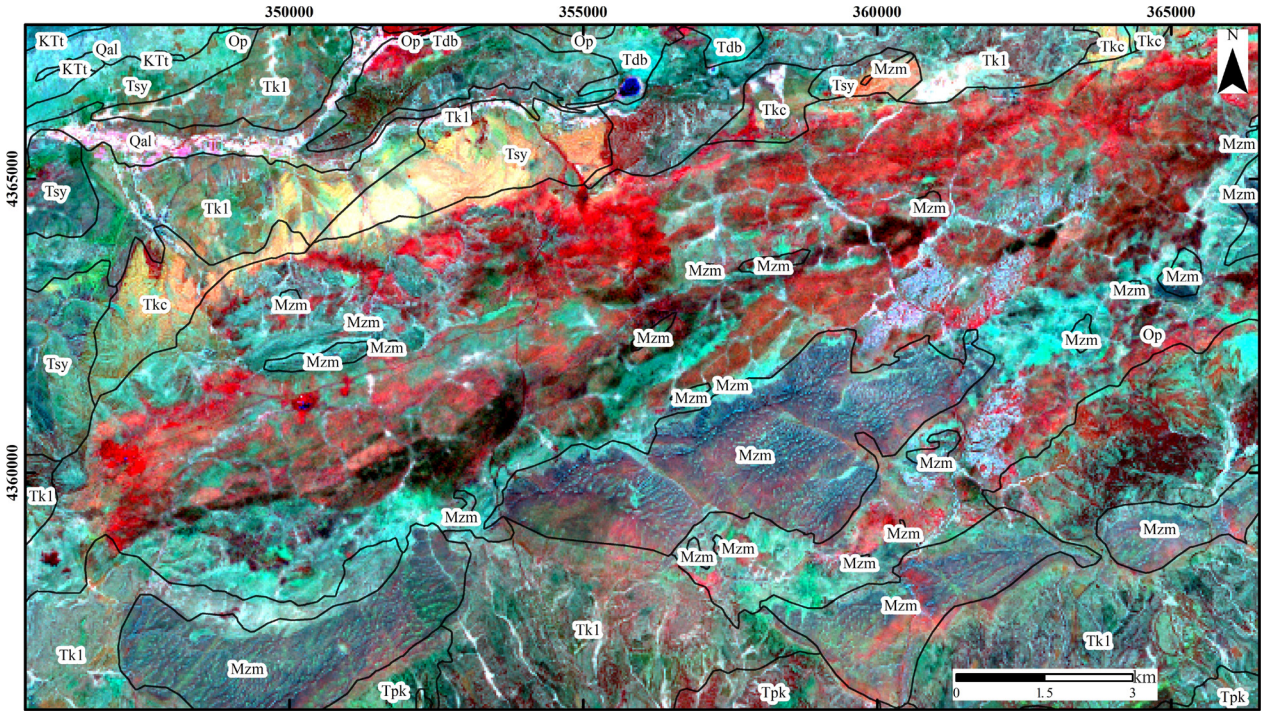

Figure 6. The band ratio image (4/8, 4/1, and 3/2*4/3 in the RGB) (abbreviations are shown in Figure 2).

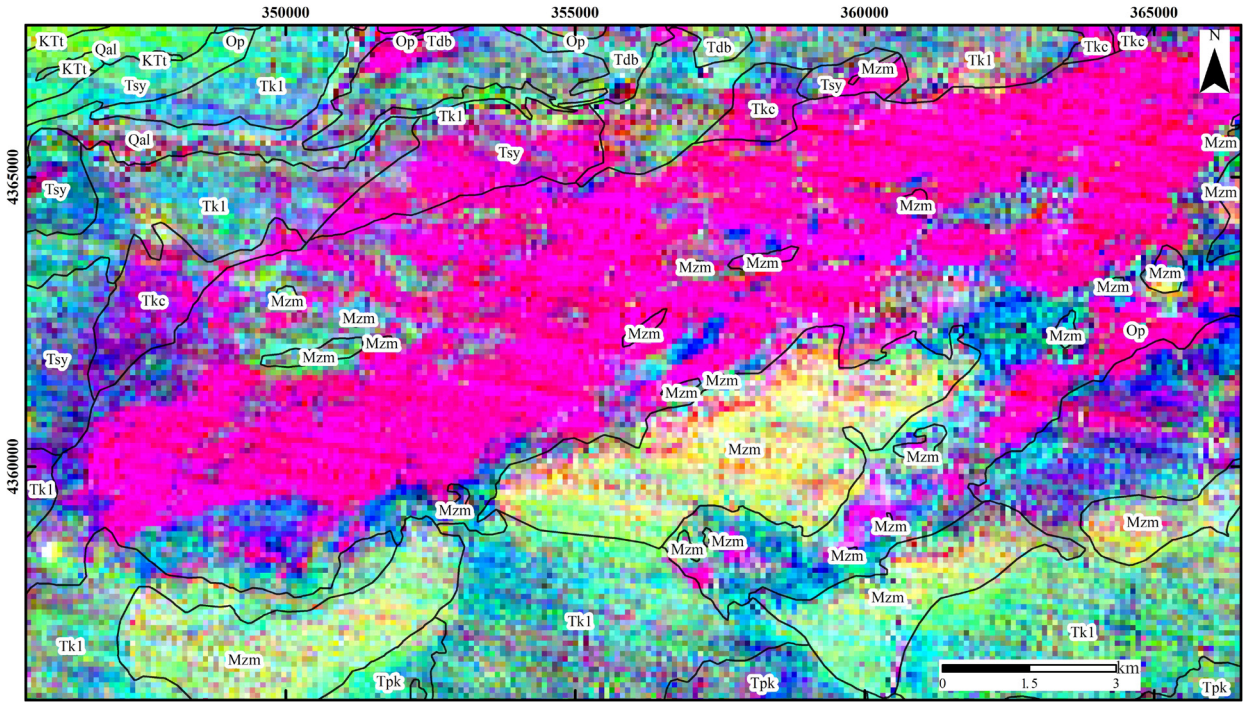

Figure 7. The false color composition of MI, CI, and QI indexes on ASTER) (abbreviations are shown in Figure 2).

of the lithological units in the study area. According to Figure 9, the ophiolites and the sedimentary rocks have been discriminated with distinct colors such as harzburgite and serpentinized dunite (greenish to reddish); limestone (dark bluish to purplish); sandstone, claystone, and siltstone (light bluish, pinkish, yellowish).

5.5. Support vector machine (SVM)

The spectral signatures of the lithological units and the water and vegetation areas have been gathered from the ASTER data according to field surveys and the geological map (Figure 10), although the spectral signatures of the lithological units are similar shapes. The differences appear in band 1, band 2, band 7, band 8, and band 9. The high reflectance of the lithological units was shown in band 3, band 4, and band 6.

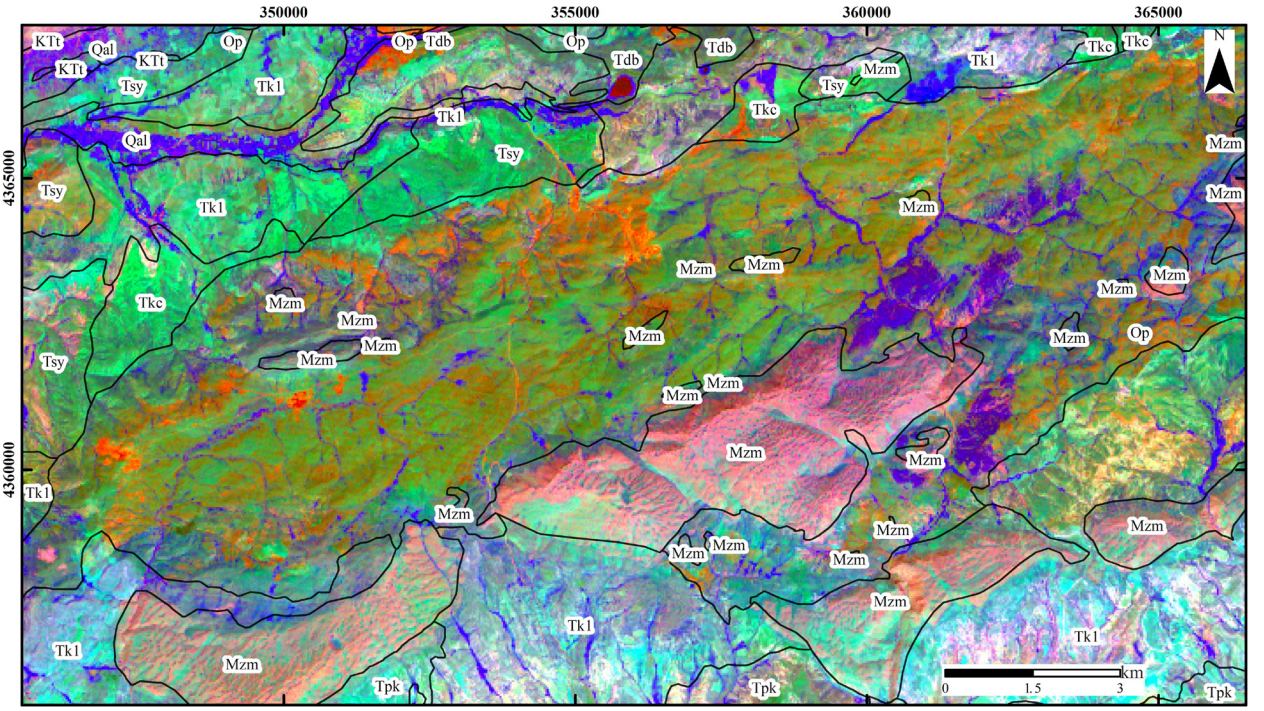

Figure 8. Decorrelation stretch result image VNIR 1-2-3 bands in the RGB (abbreviations are shown in Figure 2).

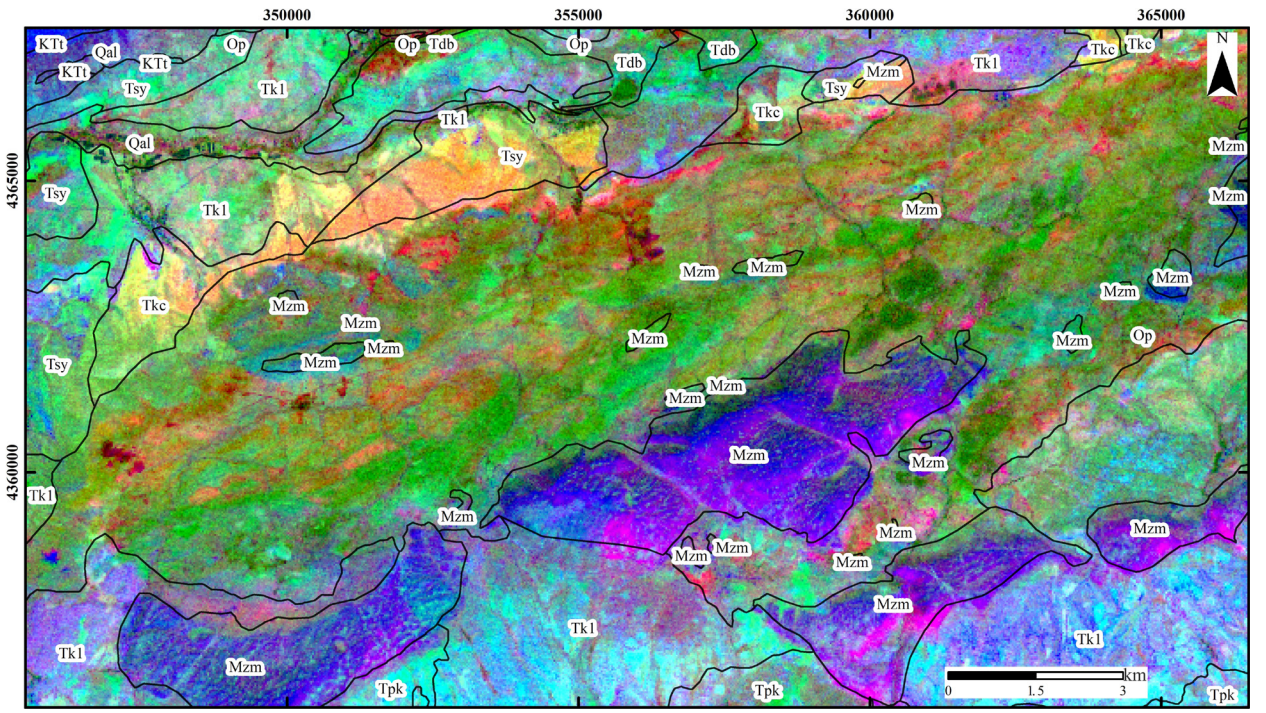

Figure 9. PCA result in the RGB (PC4, PC5, and PC1) (abbreviations are shown in Figure 2).

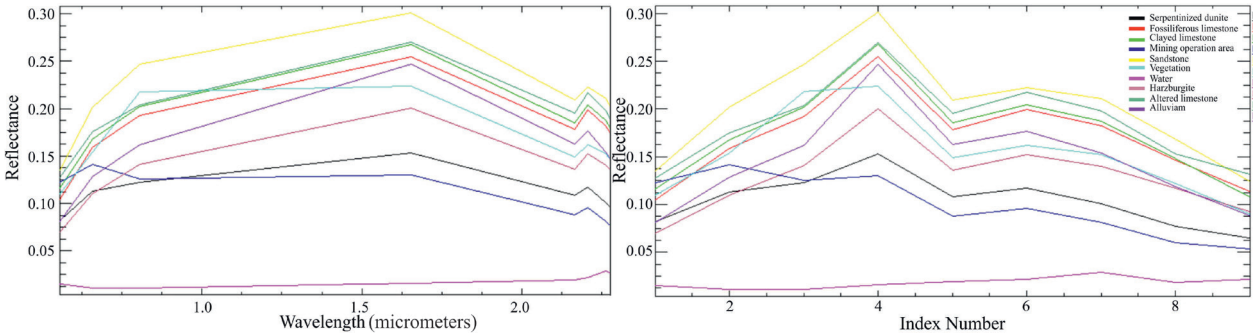

Figure 10. The spectral curves of the objects gathered from the ASTER data.

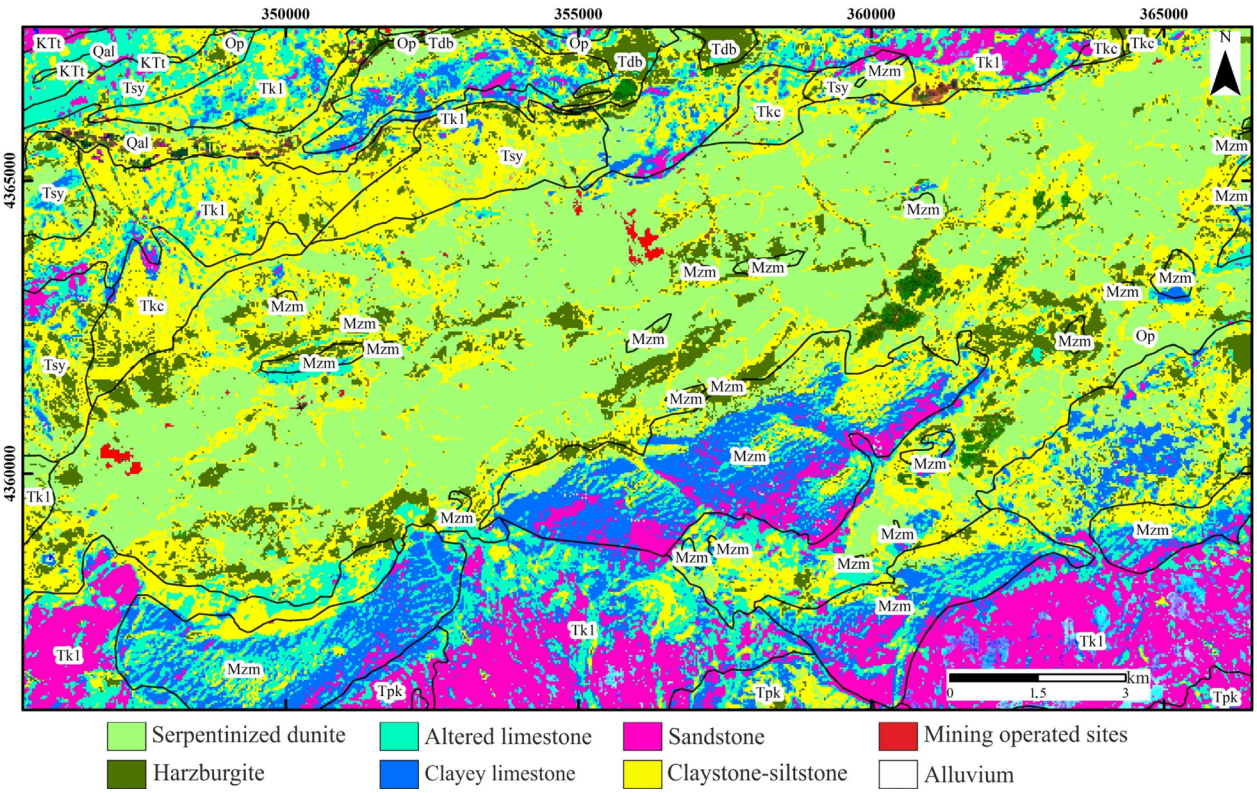

Figure 11. SVM results in the study area (abbreviations are shown in Figure 2).

Eight different lithological units including harzburgite, serpentinized dunite, sandstone, claystone-siltstone, clayey limestone, altered limestone, alluvium, and mining operation sites have been distinguished in more detail based on the geological map (Figure 11). In addition, the white pixels in the figure have been represented by water and vegetation areas.

Although the boundaries of the geological units have been outlined in the SVM results, the alluvial pixels have covered these boundaries in most areas. Therefore, field study and confirmation are required to determine the accuracy of these boundaries.

6. Conclusion

In this study, band ratios of 4/8, 4/1, and 3/2*4/3, and 9/8, 4/3, and 2/1 the PCA and DC techniques have been used to identify the ultramafic rocks of the Divriği Ophiolitic Complex and clearly distinguish them from the sedimentary rocks of the study area. The SI indices provided useful data in distinguishing between the ultramafic rocks of the Divriği Ophiolitic Complex and the sedimentary rocks of the study area. The SVM, on the other hand, has been carried out with the end members obtained from the satellite image of different rocks according to field observations, and it appears useful

results in distinguishing chromite-bearing dunites from the other ophiolite-related rock units in the area.

As a result, it is anticipated that the results obtained from this study will contribute to the mineral exploration studies to be carried out around the region in the future.

Acknowledgment
The author thanks Professor Osman Parlak (Çukurova University-Turkey), Professor Kaan Ş. Kavak, Dr. Oktay Canbaz, and Dr. Önder Gürsoy (Sivas Cumhuriyet University-Turkey) for their suggestions and scientific contributions.

References

Abdeen MM, Allison MG, Abdelsalam MG, Stern RJ (2001). Appications of ASTER band-ratio images for geological mapping in arid regions; the Neoproterozoic Allaqi Suture, Egypt. Abstract with program Geological Society of America 3: 289

Abrams M (2000). The Advanced Spaceborne Thermal Emission and Reflection Radiometer (ASTER): Data products for the high spatial resolution imager on NASA's Terra platform. International Journal Remote Sensing 21: 847-859. https://doi.org/10.1080/014311600210326

Abrams M, Hook SJ (1995). Simulated Aster Data for Geologic Studies. IEEE Transactions Geoscience Remote Sensing 33: 692–699. https://doi.org/10.1109/36.387584

Abrams MJ, Brown D, Lepley L, Sadowski R (1983). Remote sensing for porphyry copper deposits in southern Arizona. Economic Geology 78: 591–604. https://doi.org/10.2113/gsecongeo.78.4.591

Abrams MJ, Rothery DA, Pontual A (1988). Mapping in the Oman ophiolite using enhanced Landsat Thematic Mapper images. Tectonophysics 151: 387-401. https://doi.org/10.1016/0040-1951(88)90254-5

Abrams MJ, Yamaguchi Y (2019). Twenty years of ASTER contributions to lithologic mapping and mineral exploration. Remote Sensing 11: 1394. https://doi.org/DOI:10.3390/rs11111394

Ahmadi H, Kalkan K (2021). Mapping of ophiolitic complex in logar and surrounding areas (SE Afghanistan) with ASTER data. Journal of the Indian Society of Remote Sensing 49 (6): 1271-1284. https://doi.org/10.1007/s12524-021-01319-4

Aktimur T, Atalay Z, Ateş Ş, Tekirli ME, Yurdakul ME (1988). Munzur Dağları ile Çavuşdağı arasının jeolojisi. MTA Genel Müdürlüğü Raporu, No: 8320, Ankara

Aktimur T, Tekirli ME, Yurdakul ME (1990). Sivas-Erzincan Tersiyer havzasının jeolojisi. MTA Dergisi 111: 25-36

Amer R, Kusky T, Ghulam A (2010). Lithological mapping in the Central Eastern Desert of Egypt using ASTER data. Jounal of African Earth Science 56: 75-82. https://doi.org/10.1016/j.jafrearsci.2009.06.004

Archard F, D'Souza G (1994). Collection and Pre-Processing of NOAA-AVHRR 1km Resolution Data for Tropical Forest Resource Assessment. TREES Series A: Technical Report Document No: 2. European Commission, Luxembourg

Atabey E, Aktimur HT (1997). 1: 100 000 ölçekli Açınsama Nitelikli Türkiye Jeoloji Haritaları serisi, Sivas-G24 paftası, No:48. Maden Tetkik ve Arama Genel Müdürlüğü Yayını, Ankara

Bennett SA, Atkinson WW, Kruse FA (1993). Use of thematic mapper imagery to identify mineralization in the Santa Teresa District, Sonora, Mexico. International Geology Review 35: 1009-1029. https://doi.org/10.1080/00206819309465572

Beyarslan M, Bingöl AF (2000). Petrology of a suprasubduction zone ophiolite (Elazığ, Turkey). Canadian Journal of Earth Sciences 37: 1411–24. https://doi.org/10.1139/cjes-37-10-1411

Carranza EJM (2008). Geochemical Anomaly and Mineral Prospectivity Mapping in GIS. Economic Geology 104 (6): 890-890. https://doi.org/10.2113/gsecongeo.104.6.890

Chapelle O, Haffner P, Vapnik VN (1999). Support vector machines for histogram-based image classification. IEEE Transactions on Neural Networks 10 (5): 1055-1064. https://doi.org/10.1109/72.788646

Cŕosta AP, De Souza Filho CR, Azevedo F, Brodie C (2003). Targeting key alteration minerals in epithermal deposits in Patagonia, Argentina, using ASTER imagery and principal component analysis. International Journal Remote Sensing 24 (21): 4233-4240. https://doi.org/10.1080/0143116031000152291

Çelik ÖF, Delaloye M (2003). Origin of metamorphic soles and their post-kinematic mafic dyke swarms in the Antalya and Lycian ophiolites, SW Turkey. Geological Journal 38: 235–256. https://doi.org/10.1002/gj.954

Çelik ÖF, Chiaradia M, Marzoli A, Özkan M, Billor Z et al. (2013). Jurassic metabasic rocks in the Kızılırmak accretionary complex (Kargı region, Central Pontides, Northern Turkey). Tectonophysics 672: 34-49. https://doi.org/10.1016/j.tecto.2016.01.043

Çörtük RM, Çelik ÖF, Alkan A, Özkan M, Özyavaş A (2020). Distribution of rocks in Pınarbaşı Ophiolite from central Anatolia (Turkey) based on analysis of ASTER and Landsat-8 data. Geological Journal 55 (10): 6810-6822. https://doi.org/10.1002/gj.3844

Dilek Y, Furnes H (2011). Ophiolite genesis and global tectonics: Geochemical and tectonic fingerprinting of ancient oceanic lithosphere. Geological Society of American Bulletin 123 (3-4): 387-411. https://doi.org/10.1130/B30446.1

Emam A, Zoheir B, Johnson P (2016). ASTER-based mapping of ophiolitic rocks: examples from the Allaqi Heiani suture, SE Egypt. International Geology Review 58 (5): 525-539. https://doi.org/10.1080/00206814.2015.1094382

Eslami A, Ghaderi M, Rajendran A, Pour AB, Hashim M (2015). Integration of ASTER and Landsat TM satellite sensing data for chromite prospecting and lithological mapping in Neyriz ophiolite zone, south Iran. Resource Geology 65: 375-388. https://doi.org/10.1111/rge.12088

Eva H, Lambin EF (1998). Burnt area mapping in central africa using ATSR data. International Journal of Remote Sensing 19: 3473-3497. https://doi.org/10.1080/014311698213768

Floyd PA, Göncüoğlu MC, Winchester JA, Yalınız MK (2000). Geochemical character and tectonic environment of Neotethyan ophiolitic fragments and metabasites in the Central Anatolian Crystalline Complex, Turkey. In: Bozkurt, E., Winchester, J.A. & piper, J.D.A (eds), Tectonics and Magmatism in Turkey and the Surrounding Area. Geological Society, London, Special Publications 173: 183–202. https://doi.org/10.1111/rge.12088

Gabr S, Ghulam A, Kusky T (2010). Detecting areas of high potential gold mineralization using ASTER data. Ore Geology Reviews 38: 59-69. https://doi.org/10.1016/j.oregeorev.2010.05.007

Gad S, Kusky T (2007). ASTER spectral ratioing for lithological mapping in the Arabian-Nubian shield, the Neoproterozoic Wadi Kid area, Sinai, Egypt. Gondwana Research 11: 326–335. https://doi.org/10.1016/j.gr.2006.02.010

Gillespie AR, Kahle AB, Walker RE (1986). Color enhancement of highly correlated images. I Decorrelation and HSI contrast stretches. Remote Sensing Environmental 20: 209–235. https://doi.org/10.1016/0034-4257(86)90044-1

Gürsoy Ö (2019). Hybrid Band Combination for Discriminating Lithology of Dunite in Ultramafic Rocks. Journal of Indian Society Remote Sensing 47 (6): 1041-1049. https://doi.org/10.1007/s12524-019-00957-z

Hewson RD, Cudahy TJ, Huntington JF (2001). Geologic and alteration mapping at Mt Fitton, South Australia, using ASTER satellite-borne data, in: International Geoscience Remote Sensing Symposium 2: 724–726. https://doi.org/10.1109/IGARSS.2001.976615

Hewson RD, Cudahy TJ, Mizuhiko S, Ueda K, Mauger AJ (2005). Seamless geological map generation using ASTER in the Broken Hill-Curnamona province of Australia. Remote Sensing Environmental 99: 159–172. https://doi.org/10.1016/j.rse.2005.04.025

Inan S, Inan N (1988). Fasiyes özelliklerine göre Tecer kireçtaşı formasyonunu (Sivas) yapısı hakkında bir yorum. 42. Türkiye Jeoloji Kurultayı bildiri özleri, s45, Ankara

Inzana J, Kusky T, Higgs G, Tucker R (2003). Supervised classifications of Landsat TM band ratio images and Landsat TM band ratio image with radar for geological interpretations of central Madagascar. Journal of African Earth Sciences 37 (1-2): 59-72. https://doi.org/10.1016/S0899-5362(03)00071-X

Iwasakı A, Tonoka H (2005). Validation of a crosstalk correction algorithm 371 for ASTER/SIWR. Transactions Geoscience Remote Sensing 43: 2747–2751. https://doi.org/10.1109/TGRS.2005. 855066

Jensen JR (1996). Introductory Digital Image Processing: A Remote Sensing Perspective. 2nd Edition, Prentice Hall, Inc., Upper Saddle River, NJ

Kavak KŞ, Parlak O, Temiz H (2017). Geochemical characteristics of ophiolitic rocks from the southern margin of the Sivas basin and their implications for the inner Tauride Ocean, Central-Eastern Turkey. Geodinamica Acta 29 (1): 160-180. https://doi.org/10.1080/09853111.2017.1359773

Kavak KŞ, Töre Y, Temiz H, Parlak O, Çığla H et al. (2010). Differentiation of Neotethyan ophiolitic melange and an approach revealing its surficial chromite deposits using ASTER image and spectral measurements (Sivas, Turkey). Proc. SPIE 7831, Earth Resources and Environmental Remote Sensing/GIS Applications 7831: 78310D-3. https://doi.org/10.1117/12.864549

Kergaravat C (2016). Dynamique de formation et de déformation de minibassins en contexte compressif: exemple du bassin de Sivas, Turquie-Approche terrain et implications structurales multiéchelles, PhD, University of Pau, France (in French)

Khan SD, Mahmood K (2008). The application of remote sensing techniques to the study of ophiolites. Earth Science Reviews 89 (3-4): 135-143. https://doi.org/10.1016/j.earscirev.2008.04.004

Köküm M (2019). Landsat TM görüntüleri üzerinden Doğu Anadolu fay sistemi'nin Palu (Elazığ)-Pütürge (Malatya) arasındaki bölümünün çizgisellik analizi. Gümüşhane Üniversitesi Fen Bilimleri Dergisi: 9 (1): 119-127. https://doi.org/10.17714/gumusfenbil.419865

Kurtman F (1973). Sivas-Hafik-Zara ve İmranlı bölgesinin jeolojik ve tektonik yapısı. MTA Dergisi 80: 1-32

Legeay E (2017). Géodynamique du Bassin de Sivas (Turquie) - De la fermeture d'un domaine océanique à la mise en place d'un avant-pays salifère, PhD. University of Pau, France (in French)

Mohamed El-Desoky H, Soliman N, Ahmed Heikal M, Moustafa Abdel-Rahman A (2021). Mapping hydrothermal alteration zones using ASTER images in the Arabian–Nubian Shield: A case study of the northwestern Allaqi District, South Eastern Desert, Egypt. Jounal of Asian Earth Sciences 5: 100060. https://doi.org/10.1016/j.jaesx.2021.100060

Moores EM (1982). Origin and emplacement of ophiolites. Reviews of Geophysics 20 (4): 735-760. https://doi.org/10.1029/RG020i004p00735

Mosier DL, Singer DA, Moring BC, Galloway JP (2012). Podiform chromite Deposits-Database and grade and tonnage models. US Geology Survey Science. İnvestment Report, 2012 5157: 45

Ninomiya Y (2003). A Stabilized Vegetation Index and Several Mineralogic Indices Defined for ASTER VNIR and SWIR Data, in: International Geoscience and Remote Sensing Symposium (IGARSS). Proceedinds (IEEE Cat. No: 03CH37477. https://doi.org/10.1109/igarss.2003.1294172

Ninomiya Y, Fu B, Cudahy TJ (2005). Detecting lithology with Advanced Spaceborne Thermal Emission and Reflection Radiometer (ASTER) multispectral thermal infrared 'radiance-at-sensor' data. Remote Sensing Environmental 101 (4): 127-139. https://doi.org/10.1016/j.rse.2005.06.009

Okay AI, Tüysüz O (1999). Tethyan sutures of northern Turkey. Geology Society of London, Special Publications 156 (1): 475–515. https://doi.org/10.1144/GSL.SP.1999.156.01.22

Özgül N, Turşucu A, Özyardımcı N, Şenol M, Bingöl İ et al. (1981). Munzur Dağlarının Jeolojisi, MTA Derleme Raporu No: 6995 Ankara

Özgül N, Metin S, Göğer E, Bingöl İ, Baydar O et al. (1973). Tufanbeyli dolayının Kambriyen ve Tersiyer kayaları, Türkiye Jeoloji Kurultayı Bülteni 16/1: 82-100

Özkan M, Çelik ÖF, Özyavaş A (2018). Lithological discrimination of accretionary complex (Sivas, northern Turkey) using novel hybrid color composites and field data. Journal of African Earth Sciences 138: 75-85. https://doi.org/10.1016/j.jafrearsci.2017.11.009

Özkan M, Çelik ÖF, Soycan H, Çörtük RM, Marzoli A (2020). The Middle Jurassic and Early Cretaceous basalt-radiolarian chert association from the Tekelidağ Mélange, eastern İzmir-Ankara-Erzincan suture zone (northern Turkey). Cretaceous Research 107:104280. https://doi.org/10.1016/j.cretres.2019.104280

Parlak O (1996). Geochemistry and Geochronology of the Mersin Ophiolite within the Eastern Mediterranean Tectonic Frame. PhD Thesis, Terre & Environnement 6, University of Geneva, Switzerland

Parlak O, Delaloye M, Bingöl E (1996). Mineral chemistry of ultramafic and mafic cumulates as an indicator of the arc-related origin of the Mersin ophiolite (southern Turkey). Geologische Rundschau 85: 647–661. https://doi.org/10.1007/BF02440102

Parlak O, Höck V, Delaloye M (2000). Suprasubduction zone origin of the Pozantı-Karsantı ophiolite (southern Turkey) deduced from whole-rock and mineral chemistry of the gabbroic cumulates. In: Bozkurt, E., Winchester, J.A. & Piper, J.D.A (eds), Tectonics and Magmatism in Turkey and the Surrounding Area. Geological Society of London Special Publications 173: 219-234. https://doi.org/10.1144/GSL.SP.2000.173.01.11

Parlak O, Höck V, Delaloye M (2002). The supra-subduction zone Pozantı-Karsanti ophiolite, southern Turkey: evidence for high-pressure crystal fractionation of ultramafic. Lithos 65: 205-224. https://doi.org/10.1016/S0024-4937(02)00166-4

Parlak O, Höck V, Kozlu H, Delaloye M (2004). Oceanic crust generation in an island arc tectonic setting, SE Anatolian Orogenic Belt (Turkey). Geological Magazine 141: 583–603. https://doi.org/10.1017/S0016756804009458

Parlak O, Yılmaz H, Boztuğ D (2006). Origin and tectonic significance of the metamorphic sole and isolated dykes of the Divriği ophiolite (Sivas, Turkey): Evidence for a break-off prior to ophiolite emplacement. Turkish Journal of Earth Sciences 15: 25-45

Parlak O, Karaoğlan F, Rızaoğlu T, Klötzli U, Koller F et al. (2013). U-Pb and 40Ar-39Ar geochronology of the ophiolites and granitoids from the Tauride belt: implications for the evolution of the Inner Tauride suture. Journal of Geodynamics 65: 23-37. https://doi.org/10.1016/j.jog.2012.06.012

Pearce JA, Lippard SJ, Roberts S (1984). Characteristics and tectonic significance of supra subduction zone ophiolites. In: KOKELAAR, B.P. & HOWELLS, M.F. (eds), Marginal Basin Geology. Geological Society of London Special Publications 16: 77–94. https://doi.org/10.1144/GSL.SP.1984.016.01.06

Pearce JA, Geochemical fingerprinting of Oceanic Basalts with Applications to Ophiolite Classification and the Search for Archean Oceanic Crust. Lithos 100: 14-48. https://doi.org/10.1016/j.lithos.2007.06.016

Poisson A, Guezou JC, Özturk A, Inan S, Temiz H et al. (1996). Tectonic setting and evolution of the Sivas Basin, central Anatolia, Turkey. International Geology Review 38(9): 838-853. https://doi.org/10.1080/00206819709465366

Pour AB, Hashim M (2011). Identification of hydrothermal alteration minerals for exploring of porphyry copper deposit using ASTER data, SE Iran. Journal of Asian Earth Sciences 42 (6): 1309-1323. https://doi.org/10.1016/j.jseaes.2011.07.017

Pournamdari M, Hashim M, Pour AB (2014). Application of ASTER and Landsat TM data for geological mapping of esfandagheh ophiolite complex, southern Iran. Resourch Geology 64 (3): 233-246. https://doi.org/10.1111/rge.12038

Rajendran S, Al-Khirbash S, Pracejus B, Nasir S, Al-Abri AH et al. (2012). ASTER detection of chromite bearing mineralized zones in Semail Ophiolite Massifs of the northern Oman Mountains: Exploration strategy. Ore Geology Reviews 44: 121-135. https://doi.org/10.1016/j.oregeorev.2011.09.010

Rajendran S, Nasir S (2015). Mapping of Moho and Moho Transition Zone (MTZ) in Samail ophiolites of Sultanate of Oman using remote sensing technique. Tectonophysics 657: 63-80. https://doi.org/10.1016/j.tecto.2015.06.023

Rajendran S, Nasir S (2019). Mapping of hydrothermal alteration in the Late mantle-Early crust transition zone of the Tayin Massif, Sultanate of Oman using remote sensing technique. Journal of African Earth Sciences 150: 722-743. https://doi.org/10.1016/j.jafrearsci.2018.10.001

Robertson AHF (2002). Overview of the genesis and emplacement of Mesozoic ophiolites in the eastern Mediterranean Tethyan region. Lithos 65: 1-67. https://doi.org/10.1016/S0024-4937(02)00160-3

Robertson AHF (2004). Development of concepts concerning the genesis and emplacement of Tethyan ophiolites in the eastern Mediterranean and Oman regions. Earth Science Reviews 66: 331-387. https://doi.org/10.1016/j.earscirev.2004.01.005

Rothery DA (1987). Improved discrimination of rock units using Landsat Thematic Mapper imagery of the Oman ophiolite. Journal of Geology Society 144 (4): 587-597. https://doi.org/10.1144/gsjgs.144.4.0587

Rowan LC, Mars JC (2003). Lithologic mapping in the Mountain Pass, California area using Advanced Spaceborne Thermal Emission and Reflection Radiometer (ASTER) data. Remote Sensing Environmental 84: 350-366. https://doi.org/10.1016/S0034-4257(02)00127-X

Sabins FF (1987). Remote Sensing: Principles and Interpretation . By F.F.Sabins. New York: W. H. Freeman, second edition, 1986, P: 449

Sain SR, Vapnik VN (1996). The Nature of Statistical Learning Theory. Technometrics 38(4): 409. https://doi.org/10.2307/1271324

Tangestani MH, Moore F (2001). Comparison of three principal component analysis techniques to porphyry copper alteration mapping: A case study, meiduk area, (Kerman, Iran). Canadian Journal of Remote Sensing 27 (2): 176-182. https://doi.org/10.1080/07038992.2001.10854931

Thakur S, Maity D, Mondal I, Basumatary G, Ghosh PB et al. (2021). Assessment of changes in land use, land cover, and land surface temperature in the mangrove forest of Sundarbans, northeast coast of India. Environ Dev Sustain 23: 1917–1943 (2021). https://doi.org/10.1007/s10668-020-00656-7

Töre Y (2010). Sivas havzası güneydoğu kenarında yüzeylenen ofiyolitik karışığa ait birimlerin uzaktan algılama yöntemleriyle belirlenmesi. Ms, Sivas Cumhuriyet University, Sivas, Turkey (in Turkish)

Traore M, Çan T, Tekin S (2022). Mapping carbonate-hosted Pb-Zn mineralization zones in Yahyalı Province (Eastern Taurus-Turkey) using ASTER data. Advances in Space Research 69 (1): 266-281. https://doi.org/10.1016/j.asr.2021.07.034

Topuz G, Çelik OF, Şengör AMC, Altıntaş IE, Zack T et al. (2013). Jurassic ophiolite formation and emplacement as backstop to a subduction-accretion complex in northeast Turkey, the Refahiye ophiolite, and relation to the Balkan ophiolites. American Journal of Science 313: 1054-1087. https://doi.org/10.2475/10.2013.04

Url-1. (https://lpdaac.usgs.gov/data/get-started-data/collection-overview/missions/aster-overview/)

Uysal İ, Ersoy EY, Dilek Y, Escayola M, Sarıfakıoğlu E et al. (2015). Depletion and fertilization of the Tethyan oceanic Late mantle as revealed by the early Jurassic Refahiye ophiolite, NE Anatolia-Turkey. Gondwana Research 27: 594-611. https://doi.org/10.1016/j.gr.2013.09.008

Velosky JC, Stern RJ, Johnson PR (2003). Geological control of massive sulfide mineralization in the Neoproterozoic Wadi Bidah shear zone, southwestern Saudi Arabia, inferences from orbital remote sensing and field studies. Precambrian Reserch 123 (2–4): 235-247. https://doi.org/10.1016/S0301-9268(03)00070-6

Yamaguchi Y, Kahle AB, Tsu H, Kawakami T, Pniel M (1998). Overview of advanced spaceborne thermal emission and reflection radiometer (ASTER). IEEE Trans. Geoscience Remote Sensing 36: 1062-1071. https://doi.org/10.1109/36.700991

Yalınız KM, Floyd P, Göncüoğlu MC (1996). Suprasubduction zone ophiolites of Central Anatolia: geochemical evidence from the Sar›karaman ophiolite, Aksaray, Turkey. Mineralogical Magazine 60: 697-710. https://doi.org/10.1180/minmag.1996.060.402.01

Yalınız KM, Floyd P, Göncüoğlu MC (2000). Geochemistry of volcanic rocks from the Çiçekda¤ ophiolite, central Anatolia, Turkey, and their inferred tectonic setting within the northern branch of the Neotethyan ocean. In: Bozkurt, E., Winchester, J.A. & Piper, J.D.A (eds), Tectonics and Magmatism in Turkey and the Surrounding area. Geological Society of London Special Publications 173: 203-218. https://doi.org/10.1144/GSL.SP.2000.173.01.10

Yılmaz A (1989). Tectonic zones of the Caucasus and their continuations in northeastern Turkey: a correlation. Bulletin of Mineral Research and Exploration (MTA) 109: 89-106

Zabcı C (2021). Çok bantlı Landsat 8-OLI ve Sentinel-2A MSI uydu görüntülerinin karşılaştırmalı jeoloji uygulaması: Örnek çalışma alanı olarak Doğu Anadolu Fayı boyunca Palu-Hazar Gölü bölgesi (Elazığ, Türkiye). Geomatik 6 (3): 238-246. https://doi.org/10.29128/geomatik.776280

Zhang R, Zeng M (2018). Mapping lithologic components of ophiolitic Mélanges based on ASTER spectral analysis: A case study from the Bangong-Nujiang Suture Zone (Tibet, China). ISPRS International Journal of Geo-Information 7 (1): 34. https://doi.org/10.3390/ijgi7010034

Zhu G, Blumberg DG (2002). Classification using ASTER data and SVM algorithms: The case study of Beer Sheva, Israel. Remote Sensing Environment 80: 233-240. https://doi.org/10.1016/S0034- 4257(01)00305-4

Xiong Y, Khan SD, Mahmood K, Sisson VB (2011). Lithological mapping of Bela ophiolite with remote-sensing data. International journal of remote sensing 32 (16): 4641-4658. https://doi.org/10.1080/01431161.2010.489069